PNAS RESEARCH ARTICLE | CHEMISTRY MICROBIOLOGY OPEN ACCESS

Inverse stable isotope probing–metabolomics (InverSIP) identifies an iron acquisition system in a methane-oxidizing bacterial community

Jose Miguel D. Robes[a,b], Tashi C. E. Liebergesell[a,b], Delaney G. Beals[a,b,1], Xinhui Yu[a,b], William J. Brazelton[c], and Aaron W. Puri[a,b,2]

Affiliations are included on p. 9.

Edited by Alison Butler, University of California, Santa Barbara, CA; received April 4, 2025; accepted August 1, 2025

Methane is a potent greenhouse gas and a target for near-term climate change mitigation. In many natural ecosystems, methane is sequestered by microbial communities, yet little is known about how constituents of methane-oxidizing communities interact with each other and their environment. This lack of mechanistic understanding is a common issue for many important microbial communities, but it is difficult to draw links between available sequencing information and the metabolites that govern community interactions. Here, we develop and apply a technique called inverse stable isotope probing–metabolomics (InverSIP) to bridge the gap between metagenomic and metabolomic information and functionally characterize interactions in a complex methane-oxidizing community. Using InverSIP, we link a highly transcribed biosynthetic gene cluster in the community with its secondary metabolite product: methylocystabactin, a triscatecholate siderophore not previously observed in nature. We find that production of methylocystabactin is widespread among methanotrophic alphaproteobacteria and that it can be used by another methanotroph in the community that does not produce this siderophore itself. Functional assays reveal that methylocystabactin supports methanotroph growth and the activity of the methane-oxidizing enzyme soluble methane monooxygenase under conditions where bioavailable iron is limited, establishing an important molecular link between methane-oxidation and the insoluble iron found in many natural environments. These findings contribute to a molecular-level understanding of these environmentally important bacterial communities and establish InverSIP as a broadly applicable genomics-guided strategy for characterizing metabolites in microbial ecosystems.

methane | methanotroph | siderophore | stable isotope probing | metabolomics

Significance

Methane-oxidizing bacterial communities perform a critical ecosystem function by consuming this potent greenhouse gas, but the molecular mechanisms governing their activity are not well understood. We developed a genomics-guided method for studying microbial communities and used it to identify an iron-chelating secondary metabolite used by many methane-oxidizing bacteria to access iron in the environment and support methane oxidation. This work provides mechanistic details about how these environmentally important bacteria interact with their environment, which will enable the prediction and optimization of their functions from sequencing data in the future. The approaches described can also be used to characterize other microbial communities of interest that play essential roles in environmental and human health.

Methane is a powerful greenhouse gas, with a global warming potential more than 80 times that of carbon dioxide over a 20-y period (1). Due to methane's potency and relatively short half-life, it is an important target for near-term climate change mitigation (2, 3). In the environment, microbial communities provide a biotic sink for methane (4, 5). Many of these consortia contain aerobic methane-oxidizing bacteria (methanotrophs) that are metabolically linked to other bacteria that do not directly oxidize methane themselves (6, 7). Despite the critical ecosystem function of these complex communities, how the bacterial constituents interact with each other and their environment remains understudied.

Efforts to functionally characterize bacterial interactions within complex communities have lagged behind advances in sequencing-based approaches. While the accessibility of (meta)genomic sequencing data has expanded our knowledge of microbial community composition and potential function, it rarely resolves how individual members interact at a molecular level. Unlocking these mechanistic insights is critical to fully understanding how bacterial communities maintain structure, coordinate metabolic processes, and respond to environmental change.

Stable isotope probing (SIP) is one approach that helps bridge the gap between bacterial taxonomy and function by linking active metabolism to specific microbial constituents in complex communities (8, 9). In this approach, an isotopically substituted nutrient source is fed to a bacterial community, which labels metabolically active bacteria that can then be identified via metagenomic sequencing. However, while SIP can reveal metabolic linkages, it often falls short of resolving molecular-level interactions within the community, such as the production of secondary metabolites. In a variation on the SIP approach, SIP–metabolomics can be used to identify metabolites that are actively produced by members of a community (10, 11). However, in many cases, these metabolites remain as uncharacterized "dark matter" whose structure and function cannot be identified (12).

Author contributions: J.M.D.R. and A.W.P. designed research; J.M.D.R. performed research; T.C.E.L., X.Y., and W.J.B. contributed new reagents/analytic tools; J.M.D.R., T.C.E.L., D.G.B., X.Y., W.J.B., and A.W.P. analyzed data; and J.M.D.R. and A.W.P. wrote the paper.

The authors declare no competing interest.

This article is a PNAS Direct Submission.

[1]Present address: Biosciences Division, Oak Ridge National Laboratory, Oak Ridge, TN 37830.

[2]To whom correspondence may be addressed. Email: a.puri@utah.edu.

This article contains supporting information online at https://www.pnas.org/lookup/suppl/doi:10.1073/pnas.2507323122/-/DCSupplemental.

Published September 3, 2025.

Identifying secondary metabolites produced in a community can give mechanistic insight into how bacteria interact with each other and their environment. For example, iron-chelating secondary metabolites termed siderophores enable bacteria to access insoluble ferric iron (Fe^{3+}), the predominant yet poorly bioavailable form of iron in many natural environments (13, 14). Like virtually all organisms, methanotrophs need iron to grow and therefore oxidize methane, yet we do not know how these bacteria access ferric iron in the environment.

Methods have been developed to link genomic data with secondary metabolites in a so-called gene-to-molecule approach, which can provide insight into the structure and function of these molecules by adding biological context. In one example of this approach, researchers predict precursor compounds associated with a biosynthetic gene cluster (BGC) of interest, and then feed isotopically substituted versions of these precursors to identify the secondary metabolite product of the BGC (15, 16). However, isotopically substituted compounds can be difficult to obtain due to cost or lack of commercial availability. Inverse stable isotopic labeling (InverSIL) can be used to circumvent this issue by growing cultures on an isotopically substituted nutrient source and introducing unlabeled precursors of interest to trace their incorporation (17, 18). This inversion enables efficient detection of specific metabolic products without requiring isotopically labeled precursors.

Here, we combine SIP–metabolomics and InverSIL in an approach called inverse stable isotope probing–metabolomics (InverSIP) (Fig. 1). InverSIP enables the identity of actively produced metabolites to be determined by linking these compounds with their BGCs, thereby adding molecular details to the wealth of available (meta)genomic information about microbial communities. We use InverSIP to link a highly transcribed BGC with its secondary metabolite product in a complex methane-oxidizing bacterial community. We find that the secondary metabolite, which we call methylocystabactin, is a siderophore that has not previously been observed in nature and is used by methanotrophs in this community to access ferric iron. We then show that production of methylocystabactin is widespread among methanotrophic alphaproteobacteria (type II methanotrophs) and that it can be used by a related methanotroph strain from the community that does not produce methylocystabactin itself. We also show that methylocystabactin supports methanotroph growth and the activity of the enzyme soluble methane monooxygenase (sMMO) in bioavailable metal-limited cultures, thereby providing a molecular link between ferric iron and methane-oxidation. This work provides mechanistic insight into the environmental interactions of methane-oxidizing bacterial communities and establishes InverSIP as a generalizable tool to link transcribed biosynthetic genes with their secondary metabolite products in complex microbial communities.

Results

Enrichment of a Complex, Bioavailable Iron-Limited Methane-Oxidizing Bacterial Community. We enriched for a methane-oxidizing bacterial community using sediment from Lake

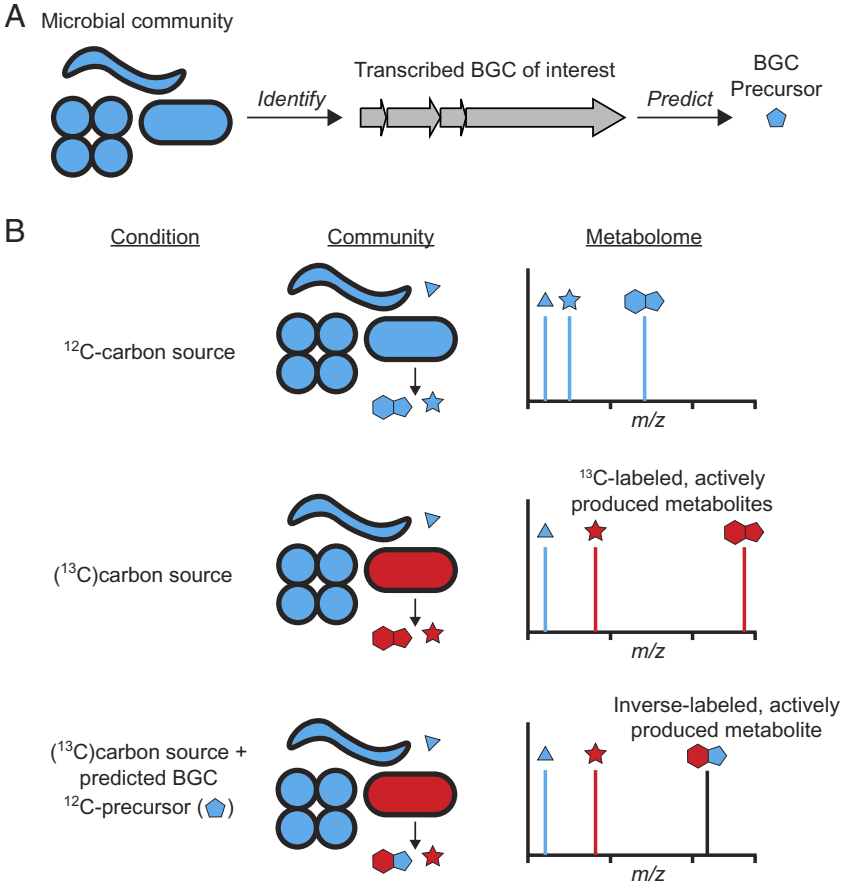

Fig. 1. Linking a transcribed BGC with its metabolite product using InverSIP. (*A*) A precursor is predicted for a transcribed BGC of interest identified in the metagenome of a microbial community. (*B*) By comparing the metabolomes of the microbial community in the presence of a carbon source at its natural isotopic abundance (referred to as ^{12}C for simplicity) and a ^{13}C-substituted carbon source [indicated as (^{13}C)], actively produced metabolites can be identified based on their *m/z* shift. An actively produced metabolite can then be linked to the BGC of interest by inverse labeling with the predicted BGC substrate. Colors indicate microbes/metabolites at their natural isotopic abundance (cyan) and ^{13}C-substituted microbes/metabolites (red).

Washington (Seattle, WA). We chose this inoculum source because its methane-oxidizing bacterial community has been well studied including using metagenomics and SIP approaches (6, 19). We used ferric iron in the enrichment culture, as bioavailable iron is often a limited resource in natural environments and is therefore a key factor in determining the structure and function of bacterial communities (14, 20). To maintain community complexity, we passaged the culture only once primarily to remove inoculum sediment.

When the enrichment reached turbidity after passaging, we analyzed the community using shotgun metagenomics. Community composition included many taxa previously observed in methane enrichments of Lake Washington sediment (19, 21). The community was complex, containing over 100 identifiable taxa at the species level (Fig. 2*A*). Methanotrophs from the families Methylococcaceae and Methylocystaceae made up 15% and 4% of the community, respectively (*SI Appendix*, Table S1). Nonmethanotrophic methylotrophs from the family Methylophilaceae (34%) were among the most abundant taxa in the culture and likely cross feed on products of methanotroph metabolism (22).

We then used shotgun metatranscriptomics to identify actively transcribed genes in the complex community. Because we are interested in secondary metabolites produced by the community, we used the BiG-MAP (BGC Meta'omics Abundance Profiler) workflow to identify transcribed BGCs (23). This led to the identification of 128 representative BGCs transcribed in at least two of the three independent enrichment replicates (*SI Appendix*, Table S2, shows top 20 BGCs).

Identification of Actively Produced Metabolites in the Community. To detect actively produced metabolites in the methane-oxidizing bacterial community, we next used SIP–metabolomics. We grew parallel enrichment cultures on ^{13}C-substituted methane [(^{13}C) methane] and methane at its natural isotopic abundance (referred to as ^{12}C-methane for simplicity) under the same conditions and for the same duration as the communities analyzed by metagenomic and metatranscriptomic sequencing. We then analyzed metabolite extracts from these conditions using untargeted, reverse-phase liquid chromatography-high-resolution tandem mass spectrometry (LC–HRMS/MS). Using an analysis workflow recently developed by our research group (24), we identified 317 unique extracellular metabolites in the ^{12}C condition and 403 unique extracellular metabolites in the ^{13}C condition (Fig. 2*B*). We further refined this to 126 high-confidence ^{12}C/^{13}C pairs that likely represent metabolites that have been actively produced in the culture. We were unable to identify any of these metabolites using common dereplication methods including Global Natural Products Social Molecular Networking (GNPS; not shown) (25).

Linking Actively Produced Metabolites to Transcribed BGCs Using InverSIP. We next attempted to use InverSIP to link actively produced metabolites with BGCs that are highly transcribed in the community. We focused on BGCs predicted to encode nonribosomal peptide synthetases, which produce peptidic secondary metabolites, for two reasons: i) many nonribosomal peptides are siderophores (26, 27), and identifying these products would therefore provide molecular details about iron acquisition in the methane-oxidizing community; and ii) the building blocks of nonribosomal peptides can often be predicted from genomic information and would be good precursors for InverSIL experiments to link BGCs with their secondary metabolites.

Most of the highly transcribed NRPS BGCs (Table 1 and *SI Appendix*, Fig. S1; see *Materials and Methods* for criteria) assembled from our short-read sequencing data were incomplete. Nonetheless, we were able to predict building blocks that were likely incorporated into several of the BGC products using adenylation domain specificity-conferring codes (28). This included the nonproteinogenic amino acid ornithine (Orn) in NRPS BGC

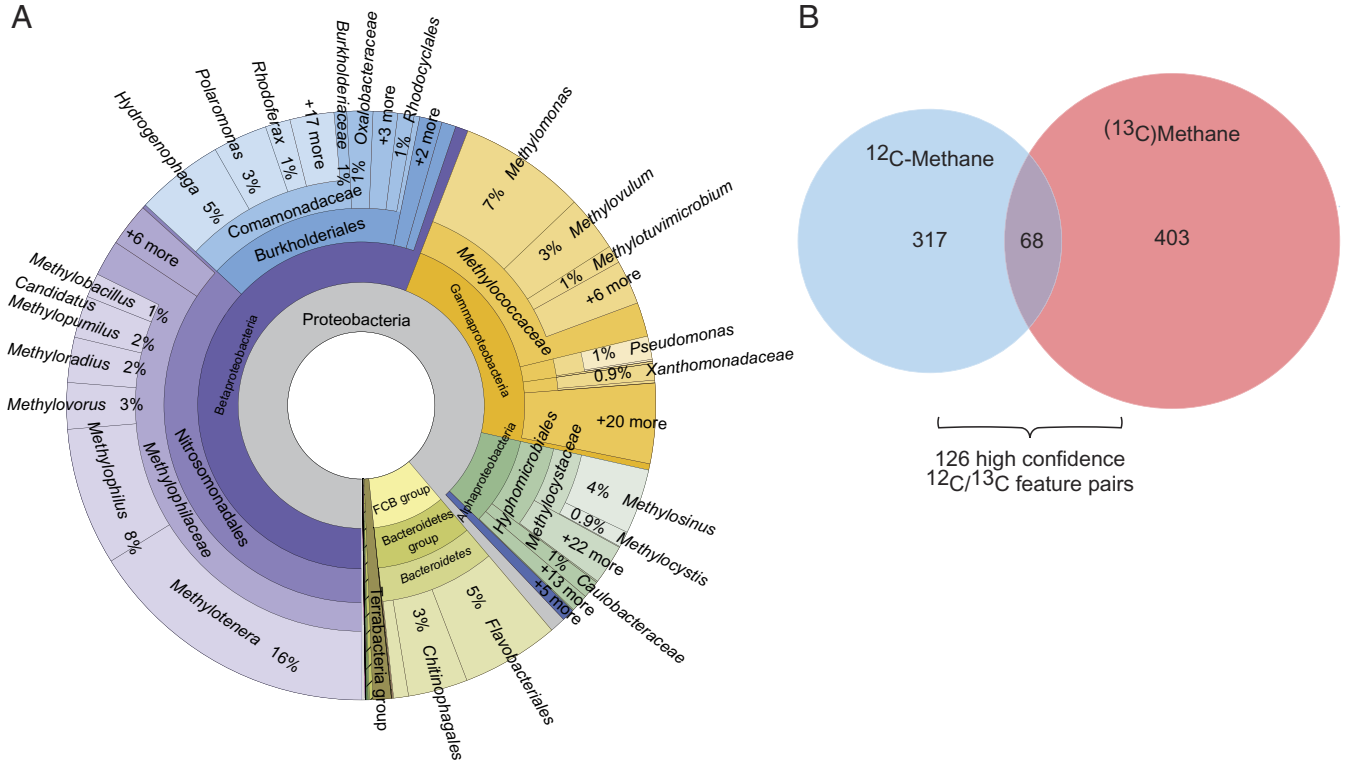

Fig. 2. A complex methane-oxidizing bacterial community enriched from Lake Washington sediment with ferric iron as the only available iron source. (*A*) Taxonomic abundances in the community metagenome. (*B*) Mass spectral features identified in the community by SIP–metabolomics.

Table 1. Highest transcribed core BGCs in the methane-oxidizing bacterial community

BGC	Full-Length BGC?	Genus	Average RPKM* (min, max)	Predicted NRPS building blocks
NRPS BGC 1	N	*Methylosinus*	3,037 (597, 5,478)	X
NRPS BGC 2	N	*Methylobacter*	2,103 (1,297, 2,910)	Leucine
NRPS BGC 3	Y	*Methylosinus*	756 (635, 877)	DHB, Serine
NRPS BGC 4	N	*Methylosinus*	642 (25, 1,259)	Ornithine
NRPS BGC 5	N	*Methylosinus*	548 (58, 1,039)	Serine

*Reads per kilobase per million mapped reads (RPKM) is reported as the average and range of the two replicates with the highest number of reads for each identified BGC. DHB: 2,3-dihydroxybenzoate.

4. Orn is an important component of many siderophore natural products, including by serving as a key chelating moiety after being modified to *N*-hydroxyornithine and further acetylated or formylated to form a hydroxamate group (29, 30). Consistent with this, NRPS BGC 4 encodes both a predicted ornithine *N*-monooxygenase and acetyltransferase, which together would be predicted to form a hydroxamate group (*SI Appendix*, Fig. S1). When we fed Orn at its natural isotopic abundance (referred to as ^{12}C-Orn for simplicity) to the ^{13}C enrichment culture, we identified an actively produced metabolite that clearly showed inverse labeling (*SI Appendix*, Fig. S2). This metabolite is a candidate for the product of NRPS BGC 4; however, we were unable to confirm this due to the incomplete nature of the BGC in the metagenome and the lack of sufficient MS/MS data to identify the presence of an *N*-hydroxyacetyl ornithine in this compound.

Next, we focused on a likely complete BGC, NRPS BGC 3, that was highly transcribed in the methane-oxidizing community (Fig. 3*A* and Table 1). This BGC was predicted to encode enzymes that synthesize a nonribosomal peptide, as well as enzymes that synthesize and activate the iron-chelating catechol 2,3-dihydroxybenzoate (DHB). The NRPS gene encodes for two modules and a thioesterase domain, which catalyzes the release of the covalently tethered product in the final step of peptide biosynthesis. We could predict that one module used serine as a substrate; however, we could not predict the amino acid incorporated by the other module. An NRPS that incorporates DHB, a potential spacer amino acid, and a serine characteristically produces a triscatecholate siderophore (31). To test this hypothesis, we fed the ^{13}C-enrichment culture ^{12}C-DHB and were able to identify a metabolite in the methane-oxidizing community that incorporated three DHB molecules (Fig. 3*B*). Using the MS/MS and inverse labeling information, we determined the planar structure of this metabolite, confirming it is indeed a triscatecholate siderophore (Fig. 3*C*).

Identification of Methylocystabactin, a Triscatecholate Siderophore Not Previously Observed in Nature. NRPS BGC 3, which we now predicted to produce a triscatecholate siderophore, was found in a metagenome-assembled genome (MAG) belonging to the *Methylosinus* genus of methane-oxidizing alphaproteobacteria (Table 1). When we searched the genomes of *Methylosinus* isolates, we found several that contained similar BGCs, including one, *Methylosinus* sp. strain LW3, that had a near-identical cluster (32, 33) (Fig. 3*A*). This strain was isolated from sediment collected at the same location as our enrichment inoculum and provided an opportunity to definitively link the BGC with its product, thereby identifying a methanotroph siderophore and confirming the utility of the InverSIP approach.

When we grew *Methylosinus* sp. strain LW3 with ferric iron as the only available iron source, we observed production of a metabolite with the same high-resolution mass, retention time, and fragmentation pattern as the metabolite identified in the enrichment culture (Fig. 3*D* and *SI Appendix*, Table S3). Further characterization of this compound by NMR and advanced Marfey's analysis confirmed that it is a cyclic triscatecholate siderophore containing a trilactone core made of *L*-serines, as well as three DHB moieties separated from the serines by glycines [(DHB-Gly-^{L}Ser)$_3$] (Fig. 3*C* and *SI Appendix*, Figs. S3–S6 and Tables S4 and S5). This siderophore was previously synthesized by Raymond and coworkers (34), and the Fe^{3+}–siderophore complex was shown to have a Λ conformation (35), which we confirmed by electronic circular dichroism (ECD) (*SI Appendix*, Fig. S7). To our knowledge, this siderophore has not previously been identified in nature.

We also performed InverSIL with ^{12}C-DHB on the *Methylosinus* sp. strain LW3 culture. We identified linear DHB-incorporating metabolites related to the main triscatecholate siderophore including linear (DHB-Gly-^{L}Ser), linear (DHB-Gly-^{L}Ser)$_2$ and linear (DHB-Gly-^{L}Ser)$_3$, as well as linear dehydrated (DHB-Gly-^{L}Ser)$_2$ and linear dehydrated (DHB-Gly-^{L}Ser)$_3$, which we inferred based on their inverse labeling patterns, MS/MS fragmentation, and a previous report characterizing dehydrated versions of the catecholate siderophore turnerbactin (36) (*SI Appendix*, Figs. S8–S14 and Table S6, see also *SI Appendix*, *Supplementary Methods*). Linear dehydrated (DHB-Gly-^{L}Ser)$_3$ has the same mass as methylocystabactin and was also detectable in the community metabolome (Fig. 3*D*).

To definitively link the siderophore with its BGC, we constructed an in-frame, unmarked deletion mutant of the *dhbA* gene in *Methylosinus* sp. strain LW3. This strain, which can no longer produce DHB, also no longer produced the siderophore (Fig. 3*D*). However, when we chemically complemented the mutant strain with DHB, it once again produced the siderophore. This confirms that the siderophore is produced by the transcribed BGC in the methane-oxidizing bacterial community and *Methylosinus* sp. strain LW3 and demonstrates the ability of InverSIP to link a transcribed BGC with its secondary metabolite product in a complex bacterial community. Furthermore, when we grew other *Methylosinus* strains as well as strains of the related *Methylocystis* genus containing similar BGCs in their genomes with ferric iron as the only iron source, they also produced the same secondary metabolite (Fig. 4*A*). We therefore name this siderophore methylocystabactin for its widespread use by members of the *Methylocystaceae* family.

Methylocystabactin Can be Used by a Nonsiderophore-producing Methanotroph from the Same Community. To determine whether methylocystabactin is the main siderophore used by *Methylosinus* sp. strain LW3 under our laboratory culture conditions, we used the chrome azurol S (CAS) assay (37). Supernatant from the *Methylosinus* sp. strain LW3 Δ*dhbA* mutant, which does not produce methylocystabactin, no longer contained a factor capable of competing with CAS for iron binding (Fig. 4*B*). This confirms that methylocystabactin is the main siderophore used by *Methylosinus* sp. strain LW3 and validates the use of the *Methylosinus* sp. strain LW3 Δ*dhbA* mutant strain for testing the importance of methylocystabactin for methanotroph physiology.

The *Methylosinus* sp. strain LW3 Δ*dhbA* mutant had a significant growth defect compared to the wild-type strain when ferric iron was the only available iron source (Fig. 4*C*). This difference

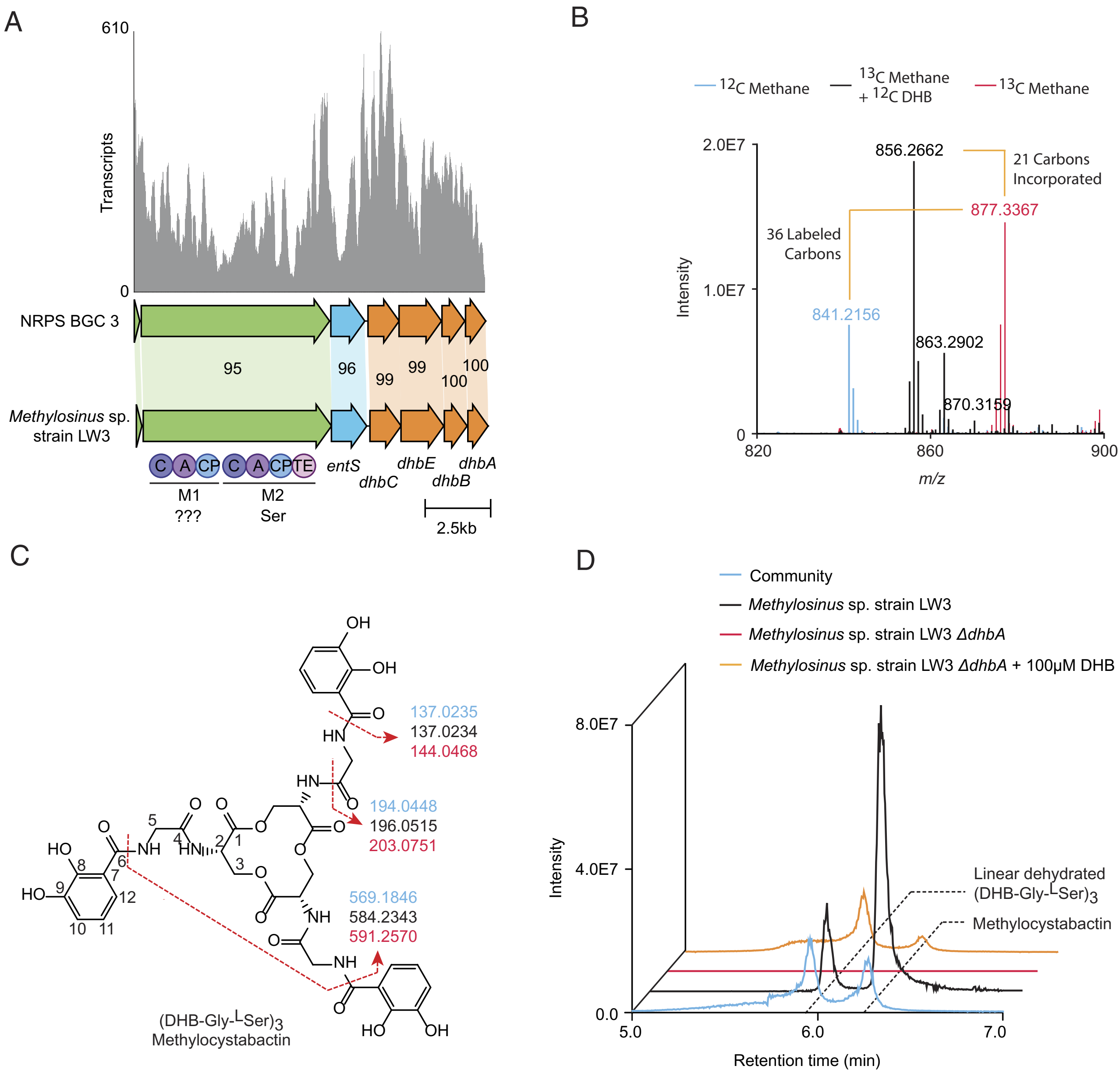

Fig. 3. Linking a highly transcribed BGC with its secondary metabolite product in the methane-oxidizing bacterial community. (*A*) Transcriptomic reads mapped to NRPS BGC 3 in the community metagenome, which has been aligned with a BGC identified in the genome of *Methylosinus* sp. strain LW3. Numbers indicate percent amino acid identity. Colors indicate a predicted NRPS gene (green), predicted siderophore exporter gene (cyan), and predicted DHB biosynthesis genes (orange). (*B*) Overlaid mass spectra showing incorporation of ^{12}C-DHB into an actively produced metabolite in the community. (*C*) Methylocystabactin structure and fragmentation from enrichments grown in ^{12}C-methane (cyan), (^{13}C)methane (red), and (^{13}C)methane + ^{12}C-DHB (black). (*D*) Extracted ion chromatograms of supernatant extracts of the listed cultures for the *m/z* value 841.2159, corresponding to the $[M + H]^+$ of methylocystabactin and linear dehydrated (DHB-Gly-^{L}Ser)$_3$. Mass tolerance < 5 ppm.

was not observed when ferric iron was replaced with bioavailable ferrous iron (Fe^{2+}). Furthermore, the growth defect was abolished when supernatant extract from the wild-type strain, which contains methylocystabactin, was added to the mutant (Fig. 4*C*). This confirms the role of methylocystabactin in ferric iron acquisition by *Methylosinus* sp. strain LW3 during growth on methane gas.

While examining the genomes of strains previously isolated from the same sediment used as inoculum for our methane-oxidizing community, we identified a strain, *Methylosinus* sp. strain LW4, that does not contain the methylocystabactin BGC in its genome (32, 33). However, this strain does have a nearly identical (97% amino acid identity) predicted TonB-dependent siderophore receptor to the one found in the methylocystabactin BGC of *Methylosinus* sp. strain LW3 (Fig. 4*D* and *SI Appendix*, Fig. S15 and Table S7, see also *SI Appendix*, *Supplementary Methods*). TonB-dependent receptors are known to play crucial roles in siderophore uptake across multiple bacterial species (13), and the co-occurrence of transporter genes with BGCs is often predictive of their function (38). This TonB-dependent receptor is most similar to the characterized receptors FatA (39), which transports the siderophore anguibactin in *Vibrio anguillarum*, and FcuA (40), which transports the siderophore ferrichrome in *Yersinia enterocolitica*. *Methylosinus* sp. strain LW4 does not produce methylocystabactin (Fig. 4*A*) or another siderophore detectable using the CAS assay (Fig. 4*B*). We therefore hypothesized that *Methylosinus* sp. strain LW4 may be able to use methylocystabactin produced by other community members (20).

To test this hypothesis, we grew *Methylosinus* sp. strain LW4 with ferric iron as the only available iron source. *Methylosinus* sp. strain LW4 had a growth defect compared to when ferric iron was replaced

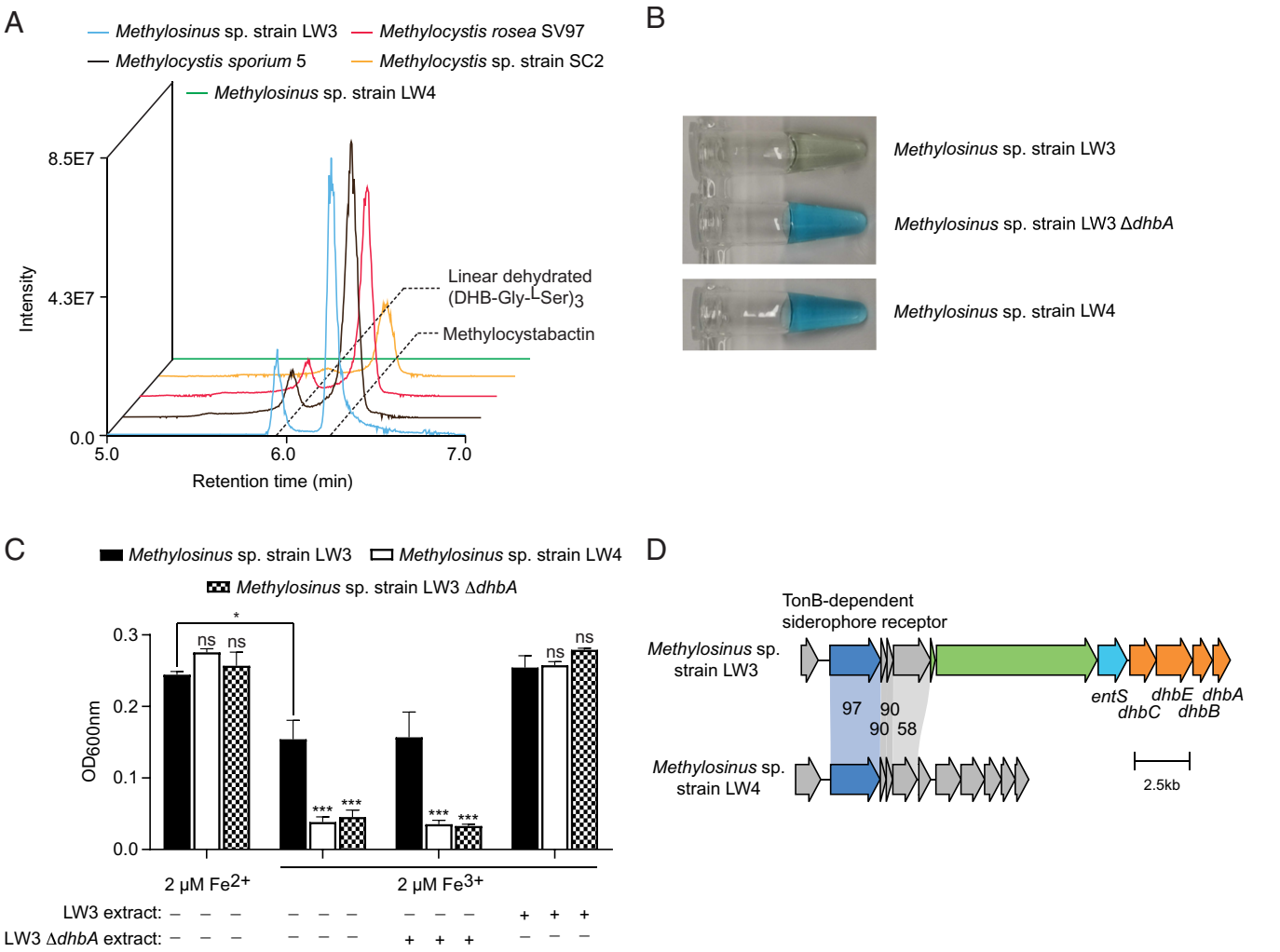

Fig. 4. Methylocystabactin enables the use of ferric iron by producing and nonproducing strains. (*A*) Extracted ion chromatograms of supernatant extracts of the listed strains grown on ferric iron for *m/z* 841.2159, corresponding to the $[M + H]^+$ of methylocystabactin and linear dehydrated (DHB-Gly-^{L}Ser)$_3$. Mass tolerance < 5 ppm. (*B*) CAS assay of supernatants from the listed strains grown on ferric iron. (*C*) Growth of the listed strains with ferrous or ferric iron measured by optical density at 600 nm (OD_{600nm}) after 3 d of incubation. Data show the mean and SD of two independent experiments with three technical replicates each. Means were compared using a one-way ANOVA with Tukey's post hoc test. OD_{600nm} values are compared to *Methylosinus* sp. strain LW3 in each growth condition unless otherwise indicated. $*P < 0.01$; $***P < 0.001$; ns, not significant. (*D*) Gene cluster comparison showing a highly similar TonB-dependent siderophore receptor in both the methylocystabactin producer *Methylosinus* sp. strain LW3 and the nonproducer *Methylosinus* sp. strain LW4. Numbers indicate percent amino acid identity. Colors indicate the predicted receptor (blue), predicted NRPS gene (green), predicted siderophore exporter gene (cyan), predicted DHB biosynthesis genes (orange), and other genes (gray).

with ferrous iron (Fig. 4*C*). However, growth of *Methylosinus* sp. strain LW4 on ferric iron was indistinguishable from *Methylosinus* sp. strain LW3 when we added methylocystabactin-containing supernatant extract from *Methylosinus* sp. strain LW3. This indicates that *Methylosinus* sp. strain LW4 can use methylocystabactin produced by other community members to access ferric iron.

Methylocystabactin Enhances the Activity of the Enzyme sMMO Under Metal-Limited Conditions. Two enzymes in methanotroph primary metabolism can oxidize methane to methanol. The main enzyme in most methanotrophs is the membrane-bound particulate methane monooxygenase (pMMO), which uses copper in its catalytic center (41). Some methanotrophs, including *Methylosinus* sp. strains LW3 and LW4, contain a cytoplasmic sMMO enzyme which uses a diiron center. In methanotrophs that contain both pMMO and sMMO, only the pMMO is highly expressed when sufficient copper is present (41). Consistent with this, we did not observe any sMMO activity when we grew *Methylosinus* sp. strain LW3, the LW3 Δ*dhbA* mutant, and *Methylosinus* sp. strain LW4 in the presence of ferric iron and copper (Fig. 5).

To determine whether methylocystabactin is important for sMMO activity under bioavailable metal-limited conditions, we also grew these strains with ferric iron and no copper. Normalized whole-cell sMMO activity was significantly lower in the LW3 Δ*dhbA* mutant and *Methylosinus* sp. strain LW4 than in wild-type *Methylosinus* sp. strain LW3 (Fig. 5). However, when we added methylocystabactin-containing supernatant extract from *Methylosinus* sp. strain LW3, both the LW3 Δ*dhbA* mutant and *Methylosinus* sp. strain LW4 sMMO activity could be increased to the level observed for *Methylosinus* sp. strain LW3 (Fig. 5). This indicates that methylocystabactin is important for these strains to oxidize the greenhouse gas methane in the absence of copper and soluble ferrous iron.

Discussion

Methane-oxidizing bacterial communities play a critical environmental role, but little is known about how community constituents interact with each other and their environment. Here, we developed and applied the technique InverSIP to link a highly

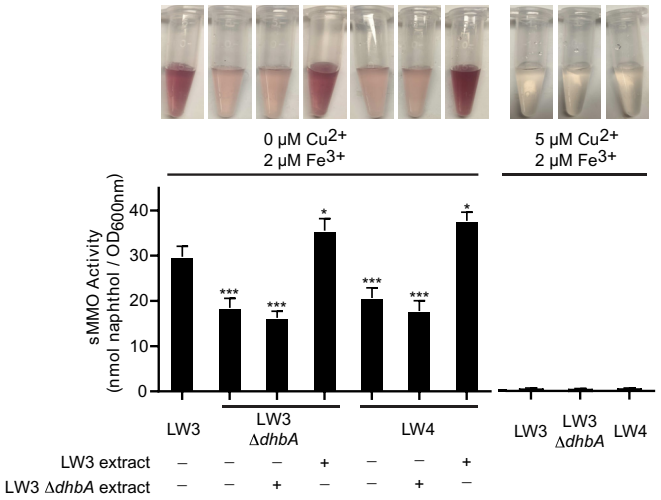

Fig. 5. Methylocystabactin is important for sMMO activity under bioavailable metal-limited conditions. Normalized whole-cell sMMO activity of *Methylosinus* sp. strain LW3, *Methylosinus* sp. strain LW3 Δ*dhbA*, and *Methylosinus* sp. strain LW4. Data show the mean and SD of two independent experiments with three technical replicates each. Pictures of the assay endpoints for each condition are shown above each bar. Means of the cultures containing 0 μM Cu^{2+} and 2 μM Fe^{3+} were compared to *Methylosinus* sp. strain LW3 under the same conditions using a one-way ANOVA with Tukey's post hoc test. **P* < 0.01; ****P* < 0.001.

transcribed BGC with its secondary metabolite product in a complex methane-oxidizing bacterial community. We found that the product is a siderophore not previously observed in nature that we named methylocystabactin, which is produced by many members of the Methylocystaceae family of methanotrophs. Methanotrophs, like virtually all organisms, need iron for growth and therefore methane-oxidation. While siderophore production has previously been reported in methanotrophs (42), to our knowledge, methylocystabactin is the first siderophore produced by a methanotroph to be structurally characterized.

A large amount of metagenomic and transcriptomic data are available for many bacterial communities of environmental or biomedical relevance. However, this information does not provide mechanistic details about bacterial interactions that shape community structure and function. Conversely, metabolomics can identify small molecules that potentially mediate such interactions, but most metabolites remain unidentified dark matter, lacking any structural annotation beyond a mass-to-charge ratio and retention time (12). Indeed, none of the actively produced metabolites in our dataset were identifiable using common dereplication pipelines such as GNPS (25). InverSIP bridges this divide by linking metabolite profiles with transcribed BGCs, enabling functional characterization of complex microbial systems.

A major advantage of InverSIP, and InverSIL approaches more broadly, is that compounds that are not easily accessible in an isotopically distinct form can be used as precursors in labeling studies. For example, to our knowledge, DHB is not currently commercially available in an isotopically substituted form, highlighting the power of using InverSIP with ^{12}C-DHB to identify methylocystabactin. InverSIL with DHB was also previously used to confirm the identity of the fimsbactin family of catecholate siderophores (43). InverSIL is well suited for discovery efforts to link transcribed biosynthetic genes to their secondary metabolite products because the precursors used often contain many isotopically distinct atoms, which results in large isotopic envelope shifts that can be readily identified using automated workflows (24). Future work using this approach will investigate additional uncharacterized BGCs in the same methane-oxidizing community.

Methylocystabactin uses a combination of amino acids to build its triscatecholate structure that have not previously been observed in nature. It shares its serine-derived trilactone core [(DHB-^{L}Ser)$_3$] with enterobactin, produced by *Escherichia coli* (31), but also contains glycine spacers (located between the trilactone core and DHB chelating moieties) similar to those found in bacillibactin [(DHB-Gly-^{L}Thr)$_3$], produced by *Bacillus* species (31). Raymond and coworkers previously synthesized methylocystabactin, which they called SERglyCAM, to compare the stereochemical conformation of its Fe^{3+}–siderophore complex to that of enterobactin and bacillibactin (35). This stereochemistry plays an important role in siderophore utilization (44, 45). The Fe^{3+}–enterobactin complex assumes a Δ conformation while both Fe^{3+}–bacillibactin and Fe^{3+}–methylocystabactin assume a Λ conformation (*SI Appendix*, Fig. S7) (35). Investigating the specificity of the methylocystabactin system will help determine whether methylocystabactin can be used by other bacterial taxa and whether methanotrophs can use these other siderophores.

We also determined that methylocystabactin can mediate interactions between members of the methane-oxidizing bacterial community. We identified a community member, *Methylosinus* sp. strain LW4, that does not produce methylocystabactin but can use this siderophore to access ferric iron for methane oxidation (Figs. 4*C* and 5). Siderophores can be considered "public goods" that are shared by community members, however, this can also lead to cheating where strains, like *Methylosinus* sp. strain LW4, use this public good without contributing to siderophore production (20). Methylocystabactin is likely therefore an important factor for the stability of this methane-oxidizing bacterial community in the presence of ferric iron, especially because triscatecholate siderophores are some of the strongest iron-chelating secondary metabolites known (13, 31).

Metals play an important role in many aspects of methanotroph primary metabolism (46). Due to the pMMO's need for copper, many methanotrophic alphaproteobacteria, including *Methylosinus* sp. strains LW3 (47) and LW4 (48), produce variants of the copper chelating secondary metabolite methanobactin (41). We have now shown that many of these same bacteria also produce methylocystabactin (Fig. 4*A*) and that when only ferric iron is available, methylocystabactin supports growth and the activity of the alternative methane monooxygenase sMMO (Fig. 5). In addition to oxidizing methane, sMMO has a broad substrate specificity and has been investigated for bioremediation of environmental contaminants (49, 50). More studies are necessary to decipher the interplay of methylocystabactin and methanobactin in the context of pMMO and sMMO regulation under various aspects of metal limitation.

Secondary metabolites often provide mechanistic links between members of microbial communities as well as between these constituents and their environment, but their functional roles remain largely unexplored. By developing and applying InverSIP, we identified methylocystabactin as a significant molecular link between commonly available ferric iron and methane-oxidation in a complex methane-oxidizing bacterial community. This highlights the power of this technique and its utility for future applications functionally characterizing interactions in other microbial communities of interest.

Materials and Methods

General Experimental Procedures. NMR spectra were obtained in CD_3OD (δH 3.34 ppm, δC 49.0 ppm) using an Agilent DirectDrive 500 with a high-sensitivity cold probe detection system. Reverse-phase HPLC was performed using an

Agilent 1260 Infinity HPLC system, and a Waters Sunfire C_{18} OBD prep column (5 μm, 10 × 100 mm) was used for purification. HPLC fractions were routinely checked for the presence of methylocystabactin using a Waters Acquity UHPLC coupled with a QDa single quadrupole mass detector and an Acquity UPLC HSS T3 C_{18} column (1.8 μm, 2.1 × 50 mm).

Strains and Bacterial Cultivation. Strains used in this study are listed in *SI Appendix*, Table S8. Pure cultures of *Methylosinus* sp. strain LW3, *Methylosinus* sp. strain LW3 *ΔdhbA*, *Methylosinus sporium* 5 (DSM17706), *Methylocystis* sp. strain SC2, and *Methylocystis rosea* SV97 were routinely grown at 30 °C in nitrate mineral salts (NMS) medium in an atmosphere of 50% (v/v) methane in air. NMS contains 0.2 g/L $MgSO_4 \cdot 7H_2O$, 0.2 g/L $CaCl_2 \cdot 6H_2O$, 1 g/L KNO_3, 30 μM $LaCl_3$, a final concentration of 5.8 mM phosphate buffer (pH 6.8), and 1X trace elements; 500X trace elements contains 1.0 g/L Na_2-EDTA, 2.0 g/L $FeSO_4 \cdot 7H_2O$, 0.8 g/L $ZnSO_4 \cdot 7H_2O$, 0.03 g/L $MnCl_2 \cdot 4H_2O$, 0.03 g/L H_3BO_3, 0.2 g/L $CoCl_2 \cdot 6H_2O$, 0.6 g/L $CuCl_2 \cdot 2H_2O$, 0.02 g/L $NiCl_2 \cdot 6H2O$, and 0.05 g/L $Na_2MoO \cdot 2H_2O$, unless the iron and/or copper species and/or concentration is otherwise indicated. Plates were grown in sealed jars, while liquid cultures were grown in 18 × 150 mm acid-washed glass tubes sealed with rubber stoppers and aluminum seals and were shaken at 200 rpm. *E. coli* strains were grown in lysogeny broth (LB) at 37 °C.

Methane Enrichment Culture. Methane enrichments were made from frozen Lake Washington sediment stored at −80 °C in 10% DMSO, which was collected from 47.63 N, 122.25 W on July 15, 2013, as part of a previous study (21). Enrichment cultures were started by adding 300 μL of thawed sediment to 6 mL of NMS diluted 1:1 with sterile ultrapure water, with the iron replaced with a final concentration of 0.1 μM $FeCl_3$. The cultures were grown with shaking in an atmosphere of 50% (v/v) methane in air at room temperature. Every 3 d, the headspace was flushed with air and new methane was added. After 10 d, this methane enrichment culture was used as the inoculum for DNA/RNA sequencing and metabolomics (InverSIP) experiments.

DNA and RNA Extraction and Sequencing. First, 5 mL of the methane enrichment culture was subdiluted into 50 mL of NMS with the iron replaced with a final concentration of 0.1 μM $FeCl_3$. These cultures were grown for 5 additional days at room temperature before nucleic acid extraction (separate cultures were used for DNA and RNA extraction). Metagenomic DNA was extracted using a FastDNA Spin Kit for Soil (MP Biomedicals), while total RNA was extracted using FastRNA Pro Soil-Direct Kit (MP Biomedicals). The total RNA was further cleaned and concentrated using an RNA Clean & Concentrator kit (ZymoResearch). Metagenomic DNA and total RNA were kept at −80 °C before submission to the Huntsman Cancer Institute–High-Throughput Genomics (HCI-HTG) shared resource at the University of Utah, where Illumina library preparation and sequencing were performed. DNA samples were prepared using a NEBNext Ultra II DNA Library Prep Kit with a 450-bp mean insert size. Total RNA samples were hybridized with NEBNext rRNA Depletion Solution to remove rRNA from the samples, and sequencing libraries were prepared using the NEBNext Ultra II RNA Library Prep Kit. Short-read Illumina sequencing was performed on an Illumina NovaSeq 6000 sequencer with 2 × 150-bp runs.

Sequencing Data Processing and Analysis. Raw metagenomic reads were trimmed using Trimmomatic (51) and were assembled using the --meta mode of SPAdes v4.0.0 (52). Each replicate was assembled individually and as a coassembly with reads from all three replicates pooled together. Metagenomic binning of each MetaSPAdes assembly was performed with the aviary pipeline (https://github.com/rhysnewell/aviary), which assesses binning results from multiple binners, including MetaBAT2 (53), VAMB (54), and SemiBin2 (55). MAGs (i.e., "bins") were also refined with DAS Tool (56) and CheckM2 (57) as part of the aviary pipeline. In addition to binning each single-replicate assembly and the coassembly, we performed a binning run including the coassembly plus contigs from the single-replicate assemblies that included BGCs of interest (defined below) that were not also identified in the coassembly.

Raw RNAseq reads were trimmed, and adapters were removed using the BBmap package from the Joint Genome Institute (https://sourceforge.net/projects/bbmap/). To map RNAseq reads with BGCs predicted from the metagenomic assembly, we used the BiG-MAP workflow (23). Briefly, BGCs were predicted on each assembly and coassembly using antiSMASH 7.0 (58) and were grouped into gene cluster families (GCF) using BiG-MAP.family.py running on default settings to remove redundancy. Metatranscriptomic reads were then mapped to each GCF using BiG-MAP.map.py to obtain an RPKM value for each GCF. BiG-MAP analysis identified and mapped 720 BGCs. BiG-MAP results were then filtered for BGCs that were transcribed in at least two replicates, and only BGCs >5,000 bp in length were further considered. Then, 128 BGCs remained, and the top 5 NRPS BGCs were manually analyzed for adenylation domain substrate prediction to select precursors for InverSIP experiments.

Community composition for the metagenomic reads was evaluated using Kaiju 1.10.1 using the nonredundant NCBI protein database (59). Kaiju results were visualized using Krona (60).

InverSIP. For each labeling condition, 600 μL of the methane enrichment culture was pelleted and resuspended in NMS with the iron replaced with a final concentration of 0.1 μM $FeCl_3$. ^{12}C-methane was added to one culture, (^{13}C)methane to another, and (^{13}C)methane plus a final concentration of 100 μM ^{12}C-precursor (DHB, *L*-ornithine) to a last culture for the labeling experiment. All cultures were grown for 5 additional days, lyophilized, and resuspended in 150 μL 50% MeOH/H_2O before analysis by LC–HRMS/MS.

LC–MS/MS data files in .raw format were converted to .mzML format using ProteoWizard's MSConvert version 3.0.23146 (61). Features were detected using MZmine version 4.1.0 (62) in the ^{12}C-medium and (^{13}C)medium conditions using the following workflow: 1) Mass detection (auto, noise level 1.5E6). 2) ADAP chromatogram builder (minimum group size 5 scans, minimum intensity for consecutive scans 2.0E6, minimum absolute height 2.0E6, *m/z* tolerance 10.0 ppm). 3) Smoothing (LOESS smoothing, Retention time width 5). 4) Local minimum feature resolver (chromatographic threshold 30.0%, minimum search range RT/Mobility 0.100, minimum relative height 10.0%, minimum absolute height 2.0E6, min ratio of peak top/edge 1.70, peak duration range 0.00 to 2.00, minimum scans 5). 5) Subsequently, isotopes were removed from ^{12}C-medium sample using the ^{13}C-isotope filter (ppm tolerance 10, retention time tolerance 0.1 min, monotonic shape required, maximum charge 3, representative isotope most intense), and the two feature tables were aligned in the order ^{12}C-medium and (^{13}C)medium conditions using the join aligner (m/z tolerance 5 ppm, weight of m/z 50, retention time tolerance 0.1 min, weight for retention time 50). The aligned feature table was exported in .csv format with the row retention time as the common element and feature m/z as the data file element.

LC–MS/MS data files in .mzML format were then converted to .h5 format using the Metabolite Atlas (available at https://github.com/biorack/metatlas) and pymzML Python packages. Next, the aligned feature table was processed along with the .h5 files for each condition using the InverSIL custom Python script (available at https://github.com/purilab/inverse). A list of 126 "high confidence" ^{12}C/^{13}C pairs were detected across all precursors. Each feature with detected labeling was then examined manually to confirm incorporation.

Growth and Extraction of Pure Methane-Oxidizing Strains for Metabolomics and InverSIL. Exponentially growing cultures of methane-oxidizing bacteria belonging to the genera *Methylosinus* and *Methlocystis* grown in NMS with ferric iron ($FeCl_3$) at a final concentration of 2 μM instead of ferrous iron were subdiluted into the same medium at an OD of 0.05. InverSIL experiments with *Methylosinus* sp. strain LW3 were set up at this point as described in the InverSIP section. After 5 d of culturing at 30 °C, the supernatant was separated from the cell pellet by centrifugation. The supernatant was then acidified with acetic acid to a final concentration of 0.1% (v/v) before being loaded onto a Discovery C_{18} solid-phase extraction (SPE) column (1 mL, 50 mg) preequilibrated with MeOH containing 0.1% (v/v) acetic acid and then sequentially eluted with 2 mL of 50%, and 100% MeOH/H_2O. Both 50 and 100% fractions were pooled and dried under nitrogen gas and reconstituted in 1 mL 50% MeOH/H_2O before analysis by LC–HRMS/MS. InverSIL data analysis was performed as described in the InverSIP section.

Ferrous and Ferric Iron Growth Studies. Wild-type *Methylosinus* sp. strain LW3, *Methylosinus* sp. strain LW3 *ΔdhbA,* and *Methylosinus* sp. strain LW4 were grown in NMS with the indicated species and concentrations of iron. To begin an experiment, exponentially growing cultures were subdiluted to an OD_{600nm} of 0.02 and DMSO or DMSO containing the dried 50% MeOH/H_2O SPE fraction from a 5-d-old culture of wild-type *Methylosinus* sp. strain LW3 or the *ΔdhbA*

mutant were added (final extract concentration 100 μg/mL). The cultures were grown for 3 d at 30 °C before measuring OD_{600nm}.

High-Resolution Tandem Mass Spectrometry (LC–HRMS/MS). Mass spectrometry data were collected using a Thermo Scientific Orbitrap Exploris 120 coupled to a Vanquish UHPLC system with an Acquity UPLC BEH C_{18} column (1.7 μm, 2.1 × 50 mm). Solvent A: Water + 0.1 % (v/v) formic acid, Solvent B: Acetonitrile + 0.1% (v/v) formic acid. The sample was eluted from the column using a 12-min linear solvent gradient: 0 to 0.1 min, 1% B; 0.1 to 10 min, 1 to 95% B. The solvent flow rate was 0.2 mL min^{-1}. Mass spectra were collected in positive ion mode, with following parameters: mass resolving power: 30,000, TopN: 4, NCE: stepped 25–35–50, isolation width: 1.5, apex trigger: on, dynamic exclusion: on, microscans: 1, isotopic exclusion: on, AGC target: standard.

Genetic Manipulation. All gene locus tags in this manuscript refer to the JGI IMG/M system (63). Genetic manipulation of *Methylosinus* sp. strain LW3 was performed as previously described (64). Sequence-verified plasmids were conjugated using the *E. coli* S17-1 donor strain (65). Plasmids and strains used are listed in *SI Appendix*, Table S8, and primers in *SI Appendix*, Table S9. Briefly, 500 μL of exponentially growing cultures of the donor and recipient strains were pelleted at 16,100 rcf for 1 min and resuspended in 500 μL sterile ultrapure water. These strains were then pelleted again, and the two pellets were combined in a total volume of 50 μL sterile ultrapure water. Next, the entire mixture was spotted onto a modified NMS agar plate containing 10% (vol/vol) nutrient broth and incubated for 2 d at 30 °C. Successful transconjugants were selected on modified NMS plates containing kanamycin (50 μg mL^{-1}). To construct the unmarked insertion mutants, kanamycin-resistant integrants (single crossovers) were restreaked and then plated on a modified NMS plate containing 1% (m/v) sucrose for counterselection. The resulting colonies were screened for double crossovers by kanamycin sensitivity and colony PCR before the final mutant was verified by Sanger sequencing.

Methylocystabactin Purification and Structure Elucidation. To isolate sufficient quantities of methylocystabactin for structural elucidation, we scaled up production and isolated methylocystabacin from *Methylosinus* sp. strain LW3 guided by LCMS and CAS assays. An exponentially growing culture of *Methylosinus* sp. strain LW3 was inoculated into 300 mL of iron-limited nitrate mineral salts in a screw-top 1 L bottle with 50% (v/v) methane in air and grown at 30 °C and 200 rpm for 5 d for a total of 15.0 L. The cell-free supernatant was obtained through centrifugation, and HP-20 Diaion resin was added, incubated, and shaken for 1 h. The resin was then collected and washed with distilled water, and crude extract was eluted sequentially from the resin using 1.0 L of 50% MeOH/H_2O and 100% MeOH. Methylocystabactin and its analogs were found in the 50% HP-20 Diaion fraction. The crude extracts containing methylocystabactin were then dried in vacuo and further fractionated by resuspension in 1 mL of 50% MeOH/H_2O and loaded onto a preequilibrated Discovery C_{18} SPE column (6 mL, 1 g) and then sequentially eluted with 15 mL of 25, 50, 75, and 100% MeOH/H_2O. Methylocystabactin and its analogs were found in the 25 and 50% MeOH/H_2O fractions. Reverse-phase HPLC purification was performed using a Sunfire C_{18} OBD column (5 μm, 10 × 100 mm) using a gradient of 20/80% to 60/40% ACN/H_2O with 0.05% trifluoroacetic acid over 20 min at 4 mL/min while continuously monitoring the eluent at 310 nm. Another reverse-phase HPLC using the same method was used to purify the compounds further (Methylocystabactin, 2.1 mg, t_R = 8.4 min)

Methylocystabactin. (DHB-Gly-^{L}Ser)$_3$. White powder; High-Resolution MS: $[M+H]^+$ calc. 841.2164, obs. 841.2159, −0.59 Δppm. NMR data: *SI Appendix*, Figs. S2–S5 and Table S4.

Determination of Amino Acid Configuration. Purified methylocystabactin (~1 mg) was hydrolyzed in 1 mL of 6 N HCl overnight at 110 °C with stirring. The solution was then evaporated to dryness, and the resulting solid was resuspended in 250 μL of water. An aliquot (50 μL) of the hydrolysate solution was then transferred to a clean glass vial to which 20 μL 1 M $NaHCO_3$ and 50 μL Marfey's reagent (L-FDLA, 1% w/v solution in acetone) were added. The mixture was stirred for 1 h at 40 °C and then quenched with 20 μL 1 N HCl. This solution was filtered and then dried before being resuspended in 50% MeOH/H_2O for UHPLC–MS analysis. The same derivatization using Marfey's reagent was done on amino acid standards. Analysis was performed on a Waters Acquity UHPLC coupled with a QDa mass detector using an Acquity UPLC HSS T3 C18 column (5/95% ACN/H_2O to 40/60% ACN/H_2O containing 0.1% formic acid, 25 min, 0.5 mL/min). Retention times for amino acids derived from methylocystabactin, and amino acids standards are summarized in *SI Appendix*, Table S5.

ECD Spectroscopy of Fe(III)-Methylocystabactin Complex. The Fe^{3+}–methylocystabactin complex for ECD analysis was prepared as previously described (35). Briefly, $FeCl_3$ was added to a stock solution of apo-methylocystabactin in DMSO to achieve an equimolar concentration of 0.1 mM in 1 mM sodium phosphate (pH 7.4). The spectra were obtained using a quartz cuvette with 1 cm path length and recorded on a Jasco J-815 spectropolarimeter. Units were converted from millidegrees (m°) to molar extinction coefficient (ε) as described previously (45) using the equation: $\varepsilon = m°/(c)(l)(32{,}980)$.

CAS Assay. CAS assay solution was prepared as previously described (37). Extracts were resuspended in 50% MeOH/H_2O and were added to the CAS assay solution to achieve a final concentration of 1 mg/mL. The reaction was incubated at room temperature for 1 h, and the resulting color changes were observed by visual inspection.

sMMO Naphthalene Assay. Wild-type *Methylosinus* sp. strain LW3, *Methylosinus* sp. strain LW3 Δ*dhbA*, and *Methylosinus* sp. strain LW4 were passaged two times in copper-free NMS. On the third passage, cells were washed and subdiluted to 0.05 OD_{600nm} in copper-free NMS with the ferrous iron replaced with ferric iron ($FeCl_3$) at a final concentration of 2 μM. DMSO or DMSO containing the dried 50% MeOH/H_2O SPE fraction from a 5-d-old culture of wild-type *Methylosinus* sp. strain LW3 or the Δ*dhbA* mutant was added (final extract concentration 100 μg/mL). The cultures were grown for 3 d at 30 °C

Whole-cell sMMO activity was monitored using a naphthalene-based assay (66, 67). In a 96-well microtiter plate, 100 μL of each culture was added in each well in triplicates, and the OD_{600nm} was measured for normalization. A saturated naphthalene solution in water was prepared, and 100 μL was added to each well. The plate was incubated for 2 h with shaking, 20 μL of freshly prepared Fast Blue B (tetrazotized o-dianisidine, 4.21 mM) was subsequently added, and the formation of the diazo dye complexes was immediately monitored at 528 nm and compared to a napthol standard curve. The intensity of the diazo dye is proportional to the concentration of naphthol produced. The specific sMMO activity was then expressed as nanomoles of naphthol formed per OD_{600nm}.

Data, Materials, and Software Availability. All metagenome and metatranscriptome sequence reads are publicly available in the NCBI via BioProject PRJNA1242065 (68). The mass spectrometry data were deposited in the public repository MassIVE via MSV000097480 (69).

ACKNOWLEDGMENTS. This work was supported by NIH Grant R35 GM147018 (to A.W.P.), NSF CAREER Award 2339190 (to A.W.P.), and Simons Foundation Early Career Investigator in Aquatic Microbial Ecology and Evolution Award SFI-LS-ECIAMEE-00006628 (to A.W.P.). T.C.E.L. was supported by NIH Training Grant T32 AI055434. We thank Z.L. Reitz (University of California, Santa Barbara) and members of the Puri Lab for helpful discussions. We thank M.E. Lidstrom (University of Washington) and J. E. Sanfilippo (University of Illinois, Urbana-Champaign) for providing feedback on the manuscript.

Author affiliations: [a]Department of Chemistry, University of Utah, Salt Lake City, UT 84112; [b]Henry Eyring Center for Cell and Genome Science, University of Utah, Salt Lake City, UT 84112; and [c]School of Biological Sciences, University of Utah, Salt Lake City, UT 84112

1. P. Forster *et al.*, "The Earth's energy budget, climate feedbacks, and climate sensitivity" in *Climate Change 2021: The Physical Science Basis: Working Group I to the Sixth Assessment Report of the Intergovernmental Panel on Climate Change* (Cambridge University Press, ed. 1, 2023).
2. K. A. Mar, C. Unger, L. Walderdorff, T. Butler, Beyond CO_2 equivalence: The impacts of methane on climate, ecosystems, and health. *Environ. Sci. Policy* **134**, 127–136 (2022).
3. I. B. Ocko *et al.*, Acting rapidly to deploy readily available methane mitigation measures by sector can immediately slow global warming. *Environ. Res. Lett.* **16**, 054042 (2021).
4. R. Cavicchioli *et al.*, Scientists' warning to humanity: Microorganisms and climate change. *Nat. Rev. Microbiol.* **17**, 569–586 (2019).

5. R. Conrad, The global methane cycle: Recent advances in understanding the microbial processes involved. *Environ. Microbiol. Rep.* **1**, 285–292 (2009).
6. M. G. Kalyuzhnaya *et al.*, High-resolution metagenomics targets specific functional types in complex microbial communities. *Nat. Biotechnol.* **26**, 1029–1034 (2008).
7. E. Hutchens, S. Radajewski, M. G. Dumont, I. R. McDonald, J. C. Murrell, Analysis of methanotrophic bacteria in Movile Cave by stable isotope probing. *Environ. Microbiol.* **6**, 111–120 (2004).
8. S. Radajewski, P. Ineson, N. R. Parekh, J. C. Murrell, Stable-isotope probing as a tool in microbial ecology. *Nature* **403**, 646–649 (2000).
9. M. G. Dumont, J. C. Murrell, Stable isotope probing–Linking microbial identity to function. *Nat. Rev. Microbiol.* **3**, 499–504 (2005).
10. R. C. Wilhelm *et al.*, Tracing carbon metabolism with stable isotope metabolomics reveals the legacy of diverse carbon sources in soil. *Appl. Environ. Microbiol.* **88**, e00839-22 (2022).
11. A. C. Mosier *et al.*, Metabolites associated with adaptation of microorganisms to an acidophilic, metal-rich environment identified by stable-isotope-enabled metabolomics. *mBio* **4**, e00484-12 (2013).
12. R. R. da Silva, P. C. Dorrestein, R. A. Quinn, Illuminating the dark matter in metabolomics. *Proc. Natl. Acad. Sci. U.S.A.* **112**, 12549–12550 (2015).
13. I. J. Schalk, Bacterial siderophores: Diversity, uptake pathways and applications. *Nat. Rev. Microbiol.* **23**, 24–40 (2025).
14. D. Emerson, E. Roden, B. Twining, The microbial ferrous wheel: Iron cycling in terrestrial, freshwater, and marine environments. *Front. Microbiol.* **3**, 383 (2012).
15. H. Gross *et al.*, The genomisotopic approach: A systematic method to isolate products of orphan biosynthetic gene clusters. *Chem. Biol.* **14**, 53–63 (2007).
16. C. S. McCaughey, J. A. Santen, J. J. J. Hooft, M. H. Medema, R. G. Linington, An isotopic labeling approach linking natural products with biosynthetic gene clusters. *Nat. Chem. Biol.* **18**, 304 (2021).
17. D. A. Cummings Jr., A. I. Snelling, A. W. Puri, Methylotroph quorum sensing signal identification by inverse stable isotopic labeling. *ACS Chem. Biol.* **16**, 1332–1338 (2021).
18. T. C. E. Liebergesell, A. W. Puri, Linking biosynthetic genes to natural products using inverse stable isotopic labeling (Inversil). *Methods Enzymol.* **702**, 215–227 (2024).
19. D. A. C. Beck *et al.*, A metagenomic insight into freshwater methane-utilizing communities and evidence for cooperation between the Methylococcaceae and the Methylophilaceae. *PeerJ* **1**, e23 (2013).
20. J. Kramer, Ö. Özkaya, R. Kümmerli, Bacterial siderophores in community and host interactions. *Nat. Rev. Microbiol.* **18**, 152–163 (2020).
21. I. Y. Oshkin *et al.*, Methane-fed microbial microcosms show differential community dynamics and pinpoint taxa involved in communal response. *ISME J.* **9**, 1119–1129 (2014).
22. S. M. B. Krause *et al.*, Lanthanide-dependent cross-feeding of methane-derived carbon is linked by microbial community interactions. *Proc. Natl. Acad. Sci. U.S.A.* **114**, 358–363 (2017).
23. V. P. Andreu *et al.*, BiG-MAP: An automated pipeline to profile metabolic gene cluster abundance and expression in microbiomes. *mSystems* **6**, e00937-21 (2021).
24. T. C. E. Liebergesell, E. G. Murdock, A. W. Puri, Detection of inverse stable isotopic labeling in untargeted metabolomic data. *Anal. Chem.* **96**, 16330–16337 (2024).
25. M. Wang *et al.*, Sharing and community curation of mass spectrometry data with Global Natural Products Social Molecular Networking. *Nat. Biotechnol.* **34**, 828–837 (2016).
26. Z. L. Reitz, M. H. Medema, Genome mining strategies for metallophore discovery. *Curr. Opin. Biotechnol.* **77**, 102757 (2022).
27. Z. L. Reitz, Predicting metallophore structure and function through genome mining. *Methods Enzymol.* **702**, 371–401 (2024).
28. T. Stachelhaus, H. D. Mootz, M. A. Marahiel, The specificity-conferring code of adenylation domains in nonribosomal peptide synthetases. *Chem. Biol.* **6**, 493–505 (1999).
29. L. Ge, S. Y. K. Seah, Heterologous expression, purification, and characterization of an l-ornithine N^5-hydroxylase involved in pyoverdine siderophore biosynthesis in Pseudomonas aeruginosa. *J. Bacteriol.* **188**, 7205–7210 (2006).
30. J. R. Heemstra, C. T. Walsh, E. S. Sattely, Enzymatic tailoring of ornithine in the biosynthesis of the *Rhizobium* cyclic trihydroxamate siderophore vicibactin. *J. Am. Chem. Soc.* **131**, 15317–15329 (2009).
31. Z. L. Reitz, M. Sandy, A. Butler, Biosynthetic considerations of triscatechol siderophores framed on serine and threonine macrolactone scaffolds. *Metallomics* **9**, 824–839 (2017).
32. A. J. Auman, S. Stolyar, A. M. Costello, M. E. Lidstrom, Molecular characterization of methanotrophic isolates from freshwater lake sediment. *Appl. Environ. Microbiol.* **66**, 5259–5266 (2000).
33. D. A. C. Beck *et al.*, Multiphyletic origins of methylotrophy in Alphaproteobacteria, exemplified by comparative genomics of Lake Washington isolates. *Environ. Microbiol.* **17**, 547–554 (2015).
34. M. E. Bluhm, S. S. Kim, E. A. Dertz, K. N. Raymond, Corynebactin and enterobactin: Related siderophores of opposite chirality. *J. Am. Chem. Soc.* **124**, 2436–2437 (2002).
35. R. J. Abergel, A. M. Zawadzka, T. M. Hoette, K. N. Raymond, Enzymatic hydrolysis of trilactone siderophores: Where chiral recognition occurs in enterobactin and bacillibactin iron transport. *J. Am. Chem. Soc.* **131**, 12682–12692 (2009).
36. A. W. Han *et al.*, Turnerbactin, a novel triscatecholate siderophore from the shipworm endosymbiont *Teredinibacter turnerae* T7901. *PLoS ONE* **8**, e76151 (2013).
37. B. Schwyn, J. B. Neilands, Universal chemical assay for the detection and determination of siderophores. *Anal. Biochem.* **160**, 47–56 (1987).
38. A. Crits-Christoph, N. Bhattacharya, M. R. Olm, Y. S. Song, J. F. Banfield, Transporter genes in biosynthetic gene clusters predict metabolite characteristics and siderophore activity. *Genome Res.* **31**, 239–250 (2021).
39. C. S. López, A. F. Alice, R. Chakraborty, J. H. Crosa, Identification of amino acid residues required for ferric-anguibactin transport in the outer-membrane receptor FatA of *Vibrio anguillarum*. *Microbiology* **153**, 570–584 (2007).
40. R. Koebnik, K. Hantke, V. Braun, The TonB-dependent ferrichrome receptor FcuA of *Yersinia enterocolitica*: Evidence against a strict co-evolution of receptor structure and substrate specificity. *Mol. Microbiol.* **7**, 383–393 (1993).
41. F. J. Tucci, A. C. Rosenzweig, Direct methane oxidation by copper- and iron-dependent methane monooxygenases. *Chem. Rev.* **124**, 1288–1320 (2024).
42. S. Yoon, A. A. Dispirito, S. M. Kraemer, J. D. Semrau, A simple assay for screening microorganisms for chalkophore production. *Methods Enzymol.* **495**, 247–258 (2011).
43. A. Proschak *et al.*, Structure and biosynthesis of fimsbactins A-F, siderophores from *Acinetobacter baumannii* and *Acinetobacter baylyi*. *ChemBioChem* **14**, 633–638 (2013).
44. J. B. Neilands, T. J. Erickson, W. H. Rastetter, Stereospecificity of the ferric enterobactin receptor of *Escherichia coli* K-12. *J. Biol. Chem.* **256**, 3831–3832 (1981).
45. P. R. Stow *et al.*, Stereospecific control of microbial growth by a combinatoric suite of chiral siderophores. *Proc. Natl. Acad. Sci. U.S.A.* **122**, e2423730122 (2025).
46. J. D. Semrau, A. A. DiSpirito, W. Gu, S. Yoon, Metals and methanotrophy. *Appl. Environ. Microbiol.* **84**, e02289-17 (2018).
47. Y. J. Park *et al.*, Characterization of a copper-chelating natural product from the methanotroph *Methylosinus* sp. LW3. *Biochemistry* **60**, 2845–2850 (2021).
48. G. E. Kenney *et al.*, Characterization of methanobactin from *Methylosinus* sp. LW4. *J. Am. Chem. Soc.* **138**, 11124–11127 (2016).
49. S.-W. Lee, D. R. Keeney, D.-H. Lim, A. A. Dispirito, J. D. Semrau, Mixed pollutant degradation by *Methylosinus trichosporium* OB3b expressing either soluble or particulate methane monooxygenase: Can the tortoise beat the hare? *Appl. Environ. Microbiol.* **72**, 7503–7509 (2006).
50. J. Colby, D. I. Stirling, H. Dalton, The soluble methane mono-oxygenase of *Methylococcus capsulatus* (Bath). Its ability to oxygenate n-alkanes, n-alkenes, ethers, and alicyclic, aromatic and heterocyclic compounds. *Biochem. J.* **165**, 395–402 (1977).
51. A. M. Bolger, M. Lohse, B. Usadel, Trimmomatic: A flexible trimmer for Illumina sequence data. *Bioinformatics* **30**, 2114–2120 (2014).
52. A. Prjibelski, D. Antipov, D. Meleshko, A. Lapidus, A. Korobeynikov, Using SPAdes de novo assembler. *Curr. Protoc. Bioinform.* **70**, e102 (2020).
53. D. D. Kang *et al.*, MetaBAT 2: An adaptive binning algorithm for robust and efficient genome reconstruction from metagenome assemblies. *PeerJ* **7**, e7359 (2019).
54. J. N. Nissen *et al.*, Improved metagenome binning and assembly using deep variational autoencoders. *Nat. Biotechnol.* **39**, 555–560 (2021).
55. S. Pan, X.-M. Zhao, L. P. Coelho, SemiBin2: Self-supervised contrastive learning leads to better MAGs for short- and long-read sequencing. *Bioinformatics* **39**, i21–i29 (2023).
56. C. M. K. Sieber *et al.*, Recovery of genomes from metagenomes via a dereplication, aggregation and scoring strategy. *Nat. Microbiol.* **3**, 836–843 (2018).
57. A. Chklovski, D. H. Parks, B. J. Woodcroft, G. W. Tyson, CheckM2: A rapid, scalable and accurate tool for assessing microbial genome quality using machine learning. *Nat. Methods* **20**, 1203–1212 (2023).
58. K. Blin *et al.*, antiSMASH 7.0: New and improved predictions for detection, regulation, chemical structures and visualisation. *Nucleic Acids Res.* **51**, W46–W50 (2023).
59. P. Menzel, K. L. Ng, A. Krogh, Fast and sensitive taxonomic classification for metagenomics with Kaiju. *Nat. Commun.* **7**, 11257 (2016).
60. B. D. Ondov, N. H. Bergman, A. M. Phillippy, Interactive metagenomic visualization in a web browser. *BMC Bioinf.* **12**, 385 (2011).
61. R. Adusumilli, P. Mallick, Data conversion with ProteoWizard msConvert. *Proteomics* **1550**, 339–368 (2017).
62. R. Schmid *et al.*, Integrative analysis of multimodal mass spectrometry data in MZmine 3. *Nat. Biotechnol.* **41**, 447–449 (2023).
63. I.-M. A. Chen *et al.*, The IMG/M data management and analysis system vol 6.0: New tools and advanced capabilities. *Nucleic Acids Res.* **49**, D751–D763 (2021).
64. S. Y. Ro, A. C. Rosenzweig, Recent advances in the genetic manipulation of *Methylosinus trichosporium* OB3b. *Methods Enzymol.* **605**, 335–349 (2018).
65. R. Simon, U. Priefer, A. Pühler, A broad host range mobilization system for in vivo genetic engineering: Transposon mutagenesis in gram negative bacteria. *Nat. Biotechnol.* **1**, 784–791 (1983).
66. D. W. Graham, D. G. Korich, R. P. LeBlanc, N. A. Sinclair, R. G. Arnold, Applications of a colorimetric plate assay for soluble methane monooxygenase activity. *Appl. Environ. Microbiol.* **58**, 2231–2236 (1992).
67. J. D. Morton, K. F. Hayes, J. D. Semrau, Effect of copper speciation on whole-cell soluble methane monooxygenase activity in *Methylosinus trichosporium* OB3b. *Appl. Environ. Microbiol.* **66**, 1730–1733 (2000).
68. J. M. D. Robes *et al.*, Sequencing data from "Inverse stable isotope probing–metabolomics (InverSIP) identifies an iron acquisition system in a methane-oxidizingbacterial community." National Center for Biotechnology Information BioProject. https://www.ncbi.nlm.nih.gov/bioproject/PRJNA1242065. Deposited 26 March 2025.
69. J. M. D. Robes *et al.*, Metabolomics data from "Inverse stable isotope probing–metabolomics (InverSIP) identifies an iron acquisition system in a methane-oxidizingbacterial community." MassIVE. https://doi.org/10.25345/C5DJ58V43. Deposited 1 April 2025.